Electronic Supplementary Material (ESI) for Physical Chemistry Chemical Physics.
This journal is © the Owner Societies 2015

Supplement 1

Experimental conditions

O_2		
Primary beam energies	*(5), 7.5, 10, 15 & 20*	*keV*
Primary beam currents	*(400,1800),2730, 3070, 3100, 2780*	*pA*
Beam dwell time per pixel	*100*	*ns*
Pixel spacing	*0.65*	*nm*
Single loop time	*98*	*ms*
Primary beam "On" time (per loop)	*18*	*ms*
Partial pressure	*2*	*mTorr*
PtC_5 deposit thickness	*100*	*nm*
Deposit thickness change	*-70*	*nm*
Number of purification loops	*7000*	*[ ]*
Purification kinetics	*top-down*	*[ ]*

H_2O		
from Journal of Physical Chemistry C 118, 14009 (2014)		
Primary beam energies	*5*	*keV*
Primary beam currents	*1000*	*pA*
Beam dwell time per pixel	*1000*	*ns*
Pixel spacing	*4*	*nm*
Single loop time	*24*	*ms*
Primary beam "On" time (per loop)	*4.4*	*ms*
Partial pressure	*75*	*mTorr*
PtC_5 deposit thickness	*60*	*nm*
Deposit thickness change	*-42*	*nm*
Number of purification loops	*2400*	*[ ]*
Purification kinetics	*bottom-up*	*[ ]*

Table S1 Select experimental conditions that provided the inspiration for the simulation results reported here.

Supplement 2

Primary electron beam scanning details

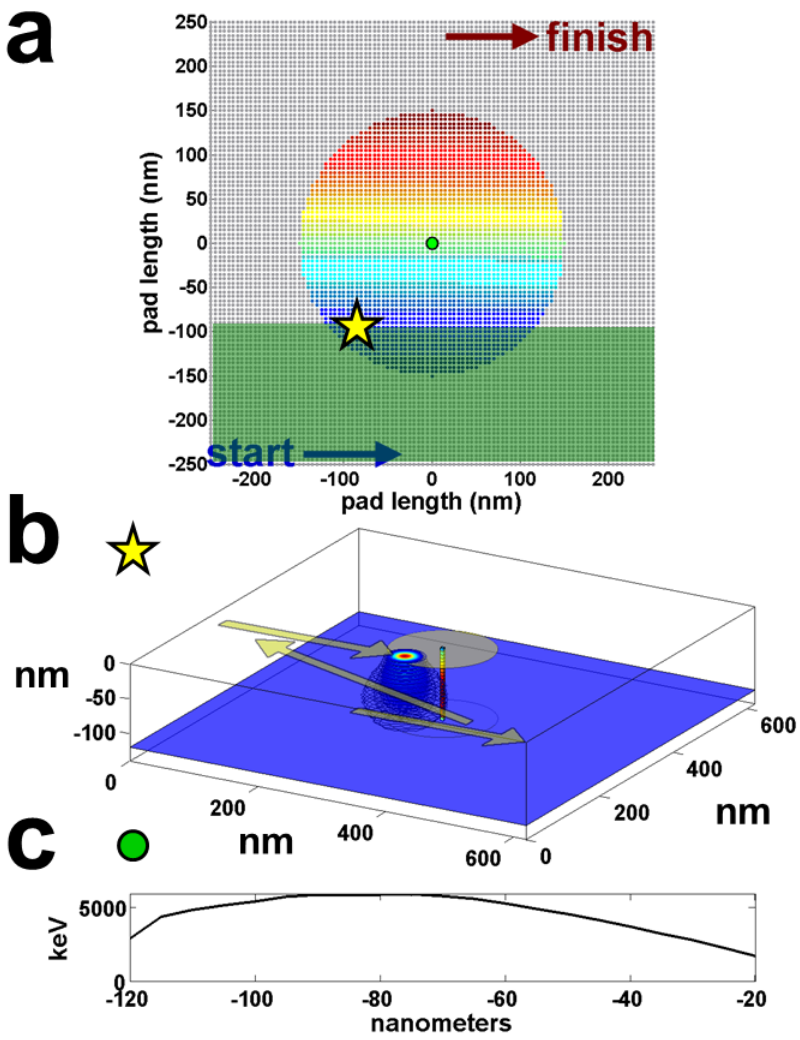

Figure S2 (a) A pixel map showing all beam dwell coordinates for a single purification loop. Each circle indicates a beam shot. The beam is "on" at each pixel during real experiments but only those shots indicated by colored coordinates contribute significant inelastic electron energy to the pixel-of-interest (POI) indicated by the green circle. The radius of this beam affected zone (BAZ) is an input parameter in the simulation. Thus, in the simulation the beam is turned on only when positioned within the BAZ. The raster pattern is indicated by the color map – the timing of shots increases from blue to red. The green overlay indicates the region already scanned (at the current snapshot in time) by the electron beam for the example of energy deposition presented in (b) with the beam currently positioned at the pixel indicated by a "star".
(b) The intersection of the electron interaction volume (5keV, FHWM=25nm) with the voxel stack of interest located at the POI. This particular beam shot is labeled in the shot map (a) with a yellow star.

Only the outer extremities of the beam insect the voxel stack shown positioned at the center of the deposit. The voxel stack below the POI is colored based on the *cumulative* amount of energy deposited there – blue represents relatively low amounts of energy while red indicates the most. The plot in (c) shows the total energy deposited as a function of energy along the voxel stack for clarity. A movie of the simulated beam dwell interaction with the voxel stack located at the POI in also provided in this Supplement.

(c) The integrated inelastic energy deposited as a function of depth into the PtC_5 deposit at the POI. All beam shots resting within the overlap of the green planar overlay, and the BAZ, in (a) have contributed energy to the voxel stack.

Supplement 3

General Reaction Model

The reviewer is correct to point out that the rate law typically used to model chemisorption is 2nd order. The expression appearing in the main text for $\partial C^{im}_O/\partial t$ describing the time–dependent concentration of immobilized, platinum bound atomic oxygen is a simplification based on the assumptions and mathematical development that follows. In general, the interaction of oxygen with a platinum nanoparticle surface (Pt_{np}) may be described by the following equations which are also shown schematically in **figure S3** along with descriptions of each reaction.

$$O_{2(dissolved)} \overset{Pt_{np}}{\rightarrow} O_{2(physisorbed)} \quad [1]$$

$$O_{2(physisorbed)} \overset{Pt_{np}}{\rightarrow} O_{(chemisorbed)} + O_{(chemisorbed)} \quad [2]$$

$$O_{(chemisorbed)} + O_{(chemisorbed)} \overset{Pt_{np}}{\rightarrow} O_{2(physisorbed)} \quad [3]$$

$$O_{2(physisorbed)} \overset{Pt_{np}}{\rightarrow} O_{2(dissolved)} \quad [4]$$

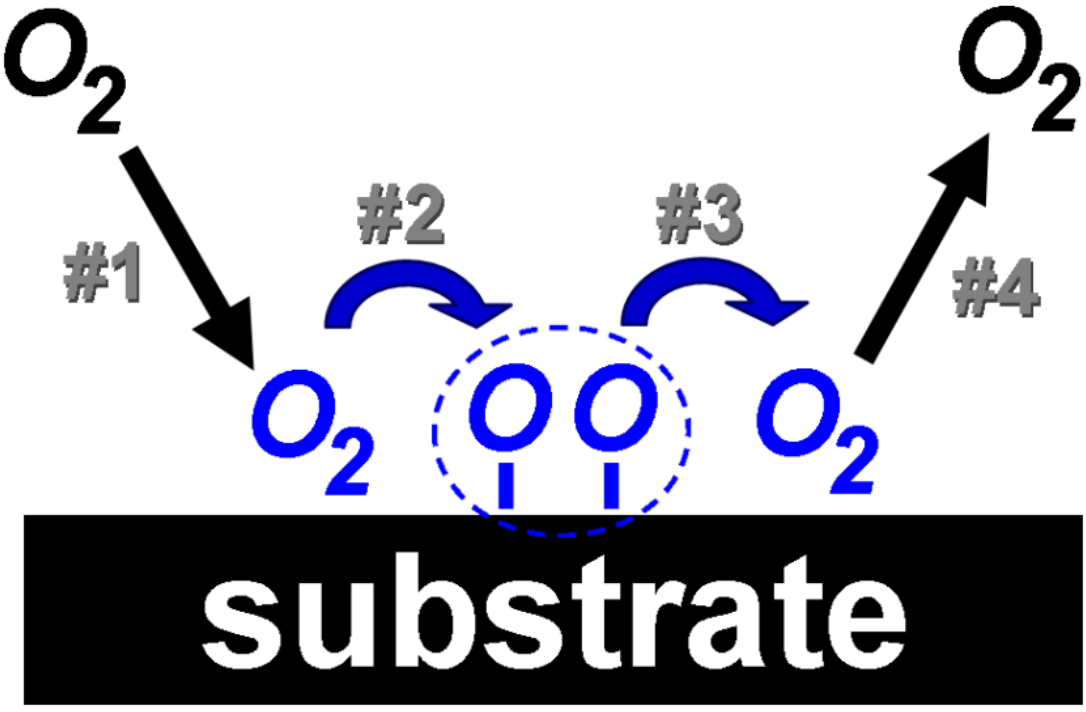

Figure S3 Oxygen gas impinges at the substrate, i.e., Pt nanoparticle surface, (#1) where a certain fraction of the incident gas physisorbs at the substrate surface. A transition between the physisorbed and chemisorbed states (#2) was assumed to occur instantly. The reverse transition (#3) from the chemisorbed state to the physisorbed state yields weakly bound physisorbed oxygen gas. Again, the physisorbed state is considered transitory. Surface desorption from the physisorbed state (#4) returns oxygen to the matrix phase (*or into the bulk for the model proposed for buried Pt nanoparticles*). The number labels in the figure are matched with the numbered equations provided above.

The general rate equations [5–8] for the reaction model provided in equations 1–4 and in **Figure S3** are;

$$\frac{\partial\left[C_{O_2}^{m}\right]}{\partial t} = D_{O_2}\frac{\partial^2 C_{O_2}^{m}}{\partial z^2} + \frac{\left[C_{O_2}^{im}\right]}{\tau_{O_2}} - \delta\Lambda_{O_2}\left(1-\theta_T\right) \quad [5]$$

$$\frac{\partial\left[C_{O_2}^{im}\right]}{\partial t} = \delta\Lambda_{O_2}\left(1-\theta_T\right) - \frac{\left[C_{O_2}^{im}\right]}{\tau_{O_2}} - k_D\left[C_{O_2}^{im}\right] + 0.5k_A\left[C_{O}^{im}\right]^2\left(1-\theta_{O_2}\right) \quad [6]$$

$$\frac{\partial\left[C_{O}^{im}\right]}{\partial t} = -k\left[C_{eV}\right]\left[C_{O}^{im}\right] + 2k_D\left[C_{O_2}^{im}\right] - k_A\left[C_{O}^{im}\right]^2\left(1-\theta_{O_2}\right) \quad [7]$$

$$\theta_T = \theta_{O_2} + \theta_O \quad [8]$$

where C^m_{O2} is the mobile concentration of O_2 diffusing in the amorphous carbon (aC), C^{im}_{O2} is the immobilized, physisorbed O_2 concentration on the Pt nanoparticle surface, C^{im}_{O} is the chemisorbed state of O bound to Pt, τ_{O2} is the mean residence time of the physisorbed O_2, k_D is the 1st order rate constant describing the dissociative chemisorption, and k_A is the 2nd order associative recombination of atomic oxygen. *Importantly, all concentrations are in units of molecules/m³, even the immobilized surface concentrations, e.g., [C^{im}_{O2}] & [C^{im}_{O}]. Typically represented in units of molecules/m², this convention of 3D spatial units, rather than 2D units, will be described in a section below*. The term Λ_{O2} is a flux term of *molecules/m³/s* and will also be described below.

The nature of the O_2 binding reaction sequence at the buried Pt interface is unknown. As a result, the binding interaction of O with Pt was reduced to a single constant (τ), defined as the mean residence time of oxygen on the nanoparticle surface, in order to avoid the complication of the multiple rate constants introduced in equations 5–7.

Simplified Reaction Model

In the model presented in the current version of the paper, O_2 has only an unbound and mobile state referenced as a concentration and referred to as C^m_{O2} in units of *molecules /m³*. The bound state of physisorbed O_2 is ignored in the current model which would otherwise be required to include the transition of physisorbed O_2 to chemisorbed O on the Pt surface (reaction #2, **Figure S3**). ***Thus, the assumption was made that (reaction #2, figure 1) proceeds instantaneously and dissolved O_2 is directly adsorbed into the chemisorbed state***. ***Moreover, (reaction #4, figure 1) is also considered to occur instantaneously relative to the other rate terms***. These combined assumptions ensure that the surface coverage of physisorbed O_2 is very low at all times. These assumptions have multiple consequences as will be developed below.

Consequences of Assumptions

One consequence of the assumptions listed above is that the coverage of physisorbed immobile O_2 tends to zero;

$$\left(1-\theta_{O_2}\right)\cong 0 \quad [9]$$

due to the transitory nature of the physisorbed O_2 state. As a result, equations 5–8 simplify to;

$$\frac{\partial\left[C^m_{O_2}\right]}{\partial t} = D_{O_2}\frac{\partial^2 C^m_{O_2}}{\partial z^2} + \frac{\left[C^{im}_{O_2}\right]}{\tau_{O_2}} - \delta\Lambda_{O_2}\left(1-\theta_O\right) \quad [10]$$

$$\frac{\partial\left[C^{im}_{O_2}\right]}{\partial t} = \delta\Lambda_{O_2}\left(1-\theta_O\right) - \frac{\left[C^{im}_{O_2}\right]}{\tau_{O_2}} - k_D\left[C^{im}_{O_2}\right] + 0.5k_A\left[C^{im}_{O}\right]^2 \quad [11]$$

$$\frac{\partial\left[C^{im}_{O}\right]}{\partial t} = -k\left[C_{eV}\right]\left[C^{im}_{O}\right] + 2k_D\left[C^{im}_{O_2}\right] - k_A\left[C^{im}_{O}\right]^2 \quad [12]$$

$$\theta_T = \theta_O \quad [13]$$

As O_2 weakly sticks to the nanoparticle surface by physisorption, the assumption is made that the transition to the chemisorbed state prevents O_2 surface accumulation during impingment according to;

$$\delta\Lambda_{O_2}\left(1-\theta_O\right) = k_D\left[C^{im}_{O_2}\right] \quad [14]$$

Likewise, the rate of depopulation of the chemisorbed *O* state to the physisorbed O_2 state should be equal to the rate of desorption of the physisorbed O_2;

$$0.5k_A\left[C_O^{im}\right]^2 = \frac{\left[C_{O_2}^{im}\right]}{\tau_{O_2}} \quad [15]$$

Substitution of equation 14 into equation 12 and substitution of equation 15 into equation 10 leads to;

$$\frac{\partial\left[C_{O_2}^{m}\right]}{\partial t} = D_{O_2}\frac{\partial^2 C_{O_2}^{m}}{\partial z^2} + 0.5k_A\left[C_O^{im}\right]^2 - \delta\Lambda_{O_2}(1-\theta_O) \quad [16]$$

$$\frac{\partial\left[C_O^{im}\right]}{\partial t} = 2\delta\Lambda_{O_2}(1-\theta_O) - k_A\left[C_O^{im}\right]^2 - k\left[C_{eV}\right]\left[C_O^{im}\right] \quad [17]$$

In order to define a 'mean residence time' for a *2nd* order reaction, a single instance of the variable $[C^{im}{}_O]$ is set as a constant $[C^{im}{}_O]_o$, in the 2nd term in equation 17, which is the mean immobilized *O* concentration integrated over an entire experiment. This development is shown below in equation 18;

$$k_A\left[C_O^{im}\right]\left[C_O^{im}\right] = \left\{k_A\left[C_O^{im}\right]_o\right\}\left[C_O^{im}\right] = \left\{\frac{1}{\tau}\right\}\left[C_O^{im}\right] \quad [18]$$

However, with this method, k_A may only be recovered <u>*after a simulation is executed*</u>. Thus, a mean residence time for atomic *O* on *Pt* is specified by τ, the simulation is executed and only then is k_A found. Thus, the value of (τ) is input into the simulation to affect the atomic *O* binding time. *This simplification has the effect of discounting O recombination during periods with large concentrations of bound O and overestimates O recombination during periods of relatively low O coverage*.

Inserting τ in place of $k_A[C^{im}{}_O]$ into equations 16–17 yields;

$$\frac{\partial\left[C_{O_2}^{m}\right]}{\partial t} = D_{O_2}\frac{\partial^2\left[C_{O_2}^{m}\right]}{\partial z^2} + 0.5\frac{\left[C_O^{im}\right]}{\tau} - \delta\Lambda_{O_2}(1-\theta_O) \quad [19]$$

$$\frac{\partial\left[C_O^{im}\right]}{\partial t} = 2\delta\Lambda_{O_2}(1-\theta_O) - \frac{\left[C_O^{im}\right]}{\tau} - k\left[C_{eV}\right]\left[C_O^{im}\right] \quad [20]$$

Bound Oxygen Concentration Conversion (2D ↔ 3D)

The volume (3D) concentration of immobile atomic oxygen is defined as;

$$\left[C_O^{im}\right] = \left[\frac{atoms}{m^3}\right] \quad [21]$$

The total number of bound O atoms per simulation voxel is;

$$\left[C_O^{im}\right] \times \Delta z^3 = \left[\frac{atoms}{m^3}\right] \times \left[\frac{m^3}{voxel}\right] = \left[\frac{atoms}{voxel}\right] \quad [22]$$

where Δz^3 is the voxel volume.

The total, mean nanoparticle surface area contained within the voxel is;

$$\rho_{np} \times 4\pi r_{np}^2 \times \Delta z^3 = \left[\frac{np}{m^3}\right] \times \left[\frac{m^2}{np}\right] \times \left[\frac{m^3}{voxel}\right] = \left[\frac{m^2}{voxel}\right] \quad [23]$$

where ρ_{np} is the average nanoparticle density in the deposit and r_{np} is the mean radius of the nanoparticle distribution. The acronym *np* indicates 'nanoparticle'. The 2D surface concentration of immobile atomic oxygen $C^{im}{}_{O(2D)}$ is related to the 3D volume concentration by dividing equation 22 by equation 23;

$$\left[C_{O(2D)}^{\ im}\right] = \frac{\left[C_O^{im}\right]\Delta z^3}{4\pi r_{np}^2 \rho_{np} \Delta z^3} = \frac{\left[C_O^{im}\right]}{4\pi r_{np}^2 \rho_{np}} = \left[\frac{atoms}{m^2}\right] \quad [24]$$

Further, the surface coverage of immobile atomic oxygen (θ_O) is simply;

$$\theta_O = \frac{\left[C_{O(2D)}^{\ im}\right]}{s_{d(O)}} = \frac{\left[C_O^{im}\right]}{4\pi r_{np}^2 \rho_{np} s_{d(O)}} \quad [25]$$

where $s_{d(O)}$ is the atomic oxygen site density on the Pt nanoparticle surface.

Mobile, Dissolved Oxygen Flux striking the Pt Nanoparticle Surface (2D ↔ 3D)

The dissolved flux of mobile O_2 that <u>sticks</u> *(δ = sticking probability upon impact which we assume is constant at low coverages*) to the nanoparticle surface area (Φ_{O2}) is;

$$\delta\Phi_{O_2} = \left[\frac{O_2}{m^2 s}\right] \quad [26]$$

Ultimately, an expression for the number of O_2 adhesion events with *Pt* surface <u>*per unit volume*</u> is needed because equations [19-20] have units of *molecules/m³/s*. Toward this aim, equation 23 is multiplied by 26 yielding;

$$\delta\Phi_{O_2} \times \rho_{np}\Delta z^3 4\pi r_{np}^2 = \left[\frac{O_2}{m^2 s}\right] \times \left[\frac{m^2}{voxel}\right] = \left[\frac{O_2}{voxel \cdot s}\right] \quad [27]$$

and subsequently dividing by the cubic voxel volume yields the expression–of–interest;

$$\delta\Phi_{O_2}\rho_{np}\Delta z^3 4\pi r_{np}^2 \times \frac{1}{\Delta z^3} = \left[\frac{O_2}{voxel \cdot s}\right] \times \left[\frac{voxel}{m^3}\right] = \delta\Phi_{O_2}\rho_{np}4\pi r_{np}^2 \left[\frac{O_2}{m^3 s}\right] \quad [28]$$

where *the number of impinging O_2 molecules on all nanoparticle surfaces contained within the voxel volume* is;

$$\Lambda_{O_2} = \Phi_{O_2}\rho_{np}4\pi r_{np}^2 \left[\frac{O_2}{m^3 s}\right] \quad [29]$$

Rate Equations for the Case of Nanoparticle Substrate

Starting from the simplified rate equations derived above and reproduced here;

$$\frac{\partial\left[C_{O_2}^m\right]}{\partial t} = D_{O_2}\frac{\partial^2\left[C_{O_2}^m\right]}{\partial z^2} + 0.5\frac{\left[C_O^{im}\right]}{\tau} - \delta\Lambda_{O_2}(1-\theta_O) \quad [19]$$

$$\frac{\partial\left[C_O^{im}\right]}{\partial t} = 2\delta\Lambda_{O_2}(1-\theta_O) - \frac{\left[C_O^{im}\right]}{\tau} - k\left[C_{eV}\right]\left[C_O^{im}\right] \quad [20]$$

the equation set is converted to the case of a substrate consisting of a nanoparticle distribution characterized by (1) a mean, dissolved nanoparticle density and (2) an average nanoparticle radius by replacing Λ_{O2} with equation 29 and θ_O with equation 25;

$$\frac{\partial\left[C_{O_2}^m\right]}{\partial t} = D_{O_2}\frac{\partial^2\left[C_{O_2}^m\right]}{\partial z^2} + 0.5\frac{\left[C_O^{im}\right]}{\tau} - \delta\Phi_{O_2}\rho_{np}4\pi r_{np}^2\left(1 - \frac{\left[C_O^{im}\right]}{4\pi r_{np}^2\rho_{np}s_{d(O)}}\right) \quad [30]$$

$$\frac{\partial\left[C_O^{im}\right]}{\partial t} = 2\delta\Phi_{O_2}\rho_{np}4\pi r_{np}^2\left(1 - \frac{\left[C_O^{im}\right]}{4\pi r_{np}^2\rho_{np}s_{d(O)}}\right) - \frac{\left[C_O^{im}\right]}{\tau} - k\left[C_{eV}\right]\left[C_O^{im}\right] \quad [31]$$

Further, $4\pi r_{np}^2\rho_{np}$ can be moved into the terms in brackets;

$$\frac{\partial\left[C_{O_2}^{m}\right]}{\partial t} = D_{O_2}\frac{\partial^2\left[C_{O_2}^{m}\right]}{\partial z^2} + 0.5\frac{\left[C_O^{im}\right]}{\tau} - \delta\Phi_{O_2}\left(\rho_{np}4\pi r_{np}^2 - \frac{\left[C_O^{im}\right]}{s_{d(O)}}\right) \quad [32]$$

$$\frac{\partial\left[C_O^{im}\right]}{\partial t} = 2\delta\Phi_{O_2}\left(\rho_{np}4\pi r_{np}^2 - \frac{\left[C_O^{im}\right]}{s_{d(O)}}\right) - \frac{\left[C_O^{im}\right]}{\tau} - k\left[C_{eV}\right]\left[C_O^{im}\right] \quad [33]$$

These equations appear in the main text as equations 5–6.

Supplement 4

Energy "Concentration" Definition

The concentration of deposited electron energy is defined as

$$\left[C_{eV}\right] = \left[\frac{eV}{m^3}\right] \quad [1]$$

This supplement is concerned with the derivation of C_{eV}. The use of the term "concentration" implies a uniform distribution of a solute dissolved in a second, homogenous phase. Under these conditions, the introduction of a cubic volume element around the concentrated region should experience a uniform flux of solute at each face. The distribution of secondary electrons (SE) generated in the bulk of a solid during the elastic scattering of primary electron trajectories emulate this criteria for three reasons. First, a significant fraction of inelastic electron energy loss goes toward the production of secondary electrons (> 10% for most materials) required to generate the "solute". Second, SEs are generated nearly randomly along any given PE trajectory granted that the selected voxel size has an edge dimesion much larger than the atomic spacing in

the crystal. In the limit of a large number of incident electrons a homogeneous and uniform distribution of SEs is created. Lastly, SEs are emitted isotropically when created such that when averaged over a large number of incident trajectories the flux of SEs entering and exiting a voxel at each face will be equal. The amorphous carbon (aC) matrix provides the homogeneous medium to support SE transport. ***Perhaps most importantly, SEs also exhibit "diffusive-like" behavior***. A conventional solute exhibits periods of directed motion followed by periods of scattering, the later due the continuous motion of the solvent. In part, an SE mimics diffusive motion owing to the fact that the SE is characterized by a mean free path (λ) a value typically a few nanometers for most materials. This provides the directed motion of the SE. The SE is either (1) absorbed into the crystal's electronic structure, (2) liberated as heat, or (3) emitted yielding the "scattering" element of diffusion. In is left as an open question as to whether heating or electron impact by way of SEs is driving the carbon oxide formation process but it is certainly related to the deposited energy liberated from the electron interaction volume. In this way, the seemingly random generation of SEs in a voxel as a large number of primary electrons pass through the voxel emulates the trajectory expected of a diffusing solute. The difference being that the random generation of the next SE by a future PE trajectory provides the next period of projected motion. **Figure S4** illustrates the concept of an SE 'concentration'.

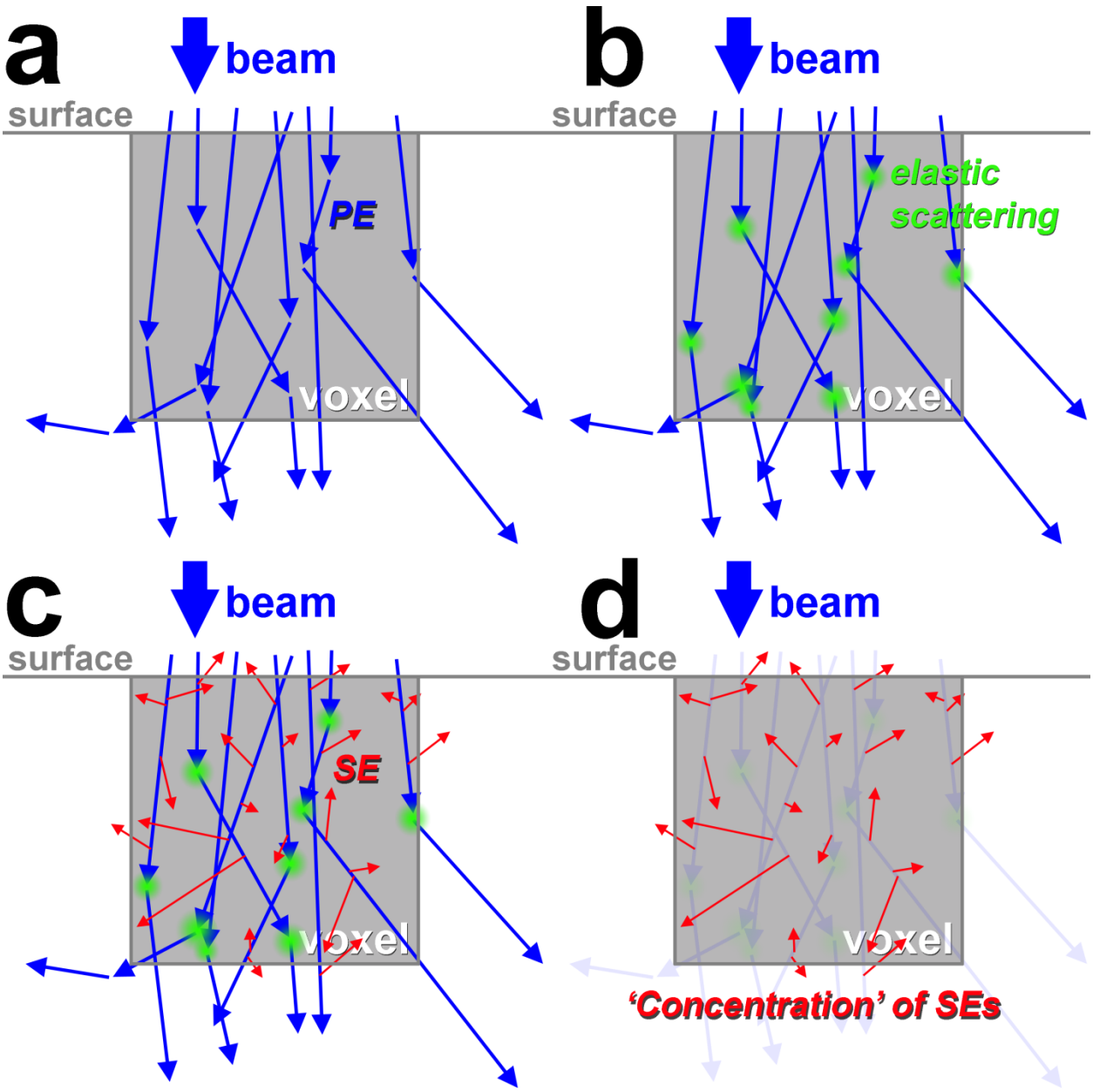

Figure S4 A schematic illustration of the sampling of multiple primary electron (PE) trajectories, shown in cross–section, as they enter a voxel intersecting the substrate surface. The PE change direction slightly, on average 3–5 degrees, due to (b) elastic scattering. In the Monte Carlo model elastic scattering occurs at discrete instances. (c) Secondary electrons (SEs) are generated effectively at random along the PE trajectories providing a homogeneous distribution on of SEs integrated over many PE trajectories. Moreover, their emission occurs in a random direction when sampling a region much larger than the atomic spacing of the underlying crystal. As a result, (d) aspects of SE transport mimic the behavior solute diffusion in a solvent.

Calculation of Energy Concentration (C_{eV})

C_{eV} is derived by tracking the 3D spatial extent of electron energy loss for a host of primary electron trajectories in the solid of interest generated using a Monte Carlo electron scattering simulation. The elastic scattering trajectory for each incident electron is overlaid with a 3D cubic voxel domain and the inelastic energy loss along the path length (s) per voxel (*dE/ds*) is tabulated using;

$$\alpha\frac{dE}{ds}\Delta s = \left[\frac{eV}{voxel}\right] \quad [2]$$

where Δs is the path length travelled by the primary electron through the current voxel in the *x*, *y* and *z* coordinates and α is a tuning parameter spanning the range (0-1) that is modulated to yield the correct number of surface emitted secondary electrons according to the secondary electron coefficient. α accounts for the fact that electron energy loss has several pathways including SE generation, bulk plasmon excitation and x–ray creation, etc. Once the correct surface emission of SEs is tuned for a given material it is assumed that the bulk emission of SEs also replicates reality. The secondary electron coefficient for PtC_5 is δ_{SE}=0.3 which required a=0.33 at a primary beam energy of E_o=5keV. δ_{SE} is calculated using;

$$\delta_{SE} = \frac{1}{n_e}\frac{\alpha}{\varepsilon}\sum_{surface\ voxels}\frac{dE}{ds}\Delta s = \left[\frac{SE}{PE}\right] \quad [3]$$

where (ε) is the energy required to create a secondary electron and (n_e) is the total number of incident primary electrons. The summation over all surface voxels is required in order to obtain δ_{SE}.

The expression *dE/ds* is the Joy and Luo modified Bethe expression for electron energy loss in the solid;

$$\frac{dE}{ds} = -78{,}500\frac{Z}{AE}ln\left(\frac{1.166(E+0.85J)}{J}\right) \quad [4]$$

and Z is the atomic number of solid, A is the atomic weight, E is the primary electron energy and J is the mean ionization potential of the solid (*Y. Lin and D. C. Joy, "A new examination of secondary electron yield data", Surface and Interface Analysis* ***37****, 895 (2005)*). Each voxel has a *Z*, *A*, and *J* based on the Pt/C ratio in the voxel.

A statistically significant total number of primary electrons (n_e) are simulation in order to produce a smooth electron energy loss distribution in the spatial coordinate. The energy loss rate for *a specific current* yields an electron inelastic energy loss spatial distribution, i.e., a power density function (P_d);

$$P_d = \frac{i_b}{q\Delta z^3}\left[\frac{1}{n_e}\sum_{n_e}\left(\int_{s_T}\frac{dE}{dS}ds\right)\right] = \left[\frac{eV}{m^3 s}\right] \quad [5]$$

where s_T is the total elastic scattering path length per electron in the solid, q is a charge of an electron and i_b is the primary beam current. In a given simulation, upon specification of i_b and the finite difference time step (Δt);

$$\left[C_{eV}\right] = P_d \Delta t \quad [6]$$

Physical Interpretation of $[C_{eV}]$

Electron beam induced etching at a vapor–substrate interface is typically represented by the following expression which presents the vertical etch rate (dh/dt) along the surface normal;

$$\frac{dh}{dt} = -\Omega_{aC} \times \sigma \times \Phi_{e^-} \times \left[C_{O(2D)}^{im}\right] = \left[\frac{m^3}{molecule}\right] \times \left[\frac{m^2}{e^-}\right] \times \left[\frac{e^-}{m^2 s}\right] \times \left[\frac{molecules}{m^2}\right] = \left[\frac{m}{s}\right] \quad [5]$$

The atomic volume of amorphous carbon (Ω_{aC}), the electron impact dissociation cross–section for a surface adsorbed etchant molecule (σ), the incident electron flux at the surface (Φ_{e^-}) and the surface (2D) concentration of adsorbed etchant, in this example atomic O, [$C^{im}_{O(2D)}$] all effect the etch rate.

In the model presented in this work, the consumption of amorphous carbon is treated using a 2nd order reaction rate model of the form;

$$\frac{\partial[aC]}{\partial t} = -\frac{2}{3} \times k \times \left[C_{eV}\right] \times \left[C_O^{im}\right] = \left[\frac{aC}{O}\right] \times \left[\frac{m^3}{eV\ s}\right] \times \left[\frac{eV}{m^3}\right] \times \left[\frac{O}{m^3}\right] = \left[\frac{aC}{m^3\ s}\right] \quad [6]$$

and the *2/3* factor accounts for the fact that *2/3C atoms (from the amorphous matrix)* is liberated per *O* when the average reaction by–product is $CO_{1.5}$. This *2/3* factor will be dropped in the following development in order to focus on the relationship between σ and k. Equation 6 can be converted to an etched volume;

$$\frac{\partial\left([aC]\Delta z^3 \Omega_{aC}\right)}{\partial t} = \frac{\partial V_{aC}}{\partial t} = -k\left[C_{eV}\right]\left[C_O^{im}\right]\Delta z^3 \Omega_{aC} = \left[\frac{m^3}{s}\right] \quad [6]$$

Similarly, equation 5 can also be converted in a volumetric etch rate;

$$\frac{d(h\Delta z^2)}{dt} = -\Omega_{aC}\sigma\Phi_{e^-}\left[C_{O(2D)}^{im}\right]\Delta z^2 = \left[\frac{m^3}{s}\right] \quad [7]$$

Multiplying the right hand side by $\Delta z/\Delta z$ makes it possible to convert $[C^{im}_{O(2D)}]$ into $[C^{im}_{O}]$;

$$\frac{dV_{aC}}{dt} = -\Omega_{aC}\sigma\Phi_{e^-}\left[C_{O(2D)}^{im}\right]\Delta z^2\frac{\Delta z}{\Delta z} = -\Omega_{aC}\sigma\Phi_{e^-}\frac{\left[C_{O(2D)}^{im}\right]}{\Delta z}\Delta z^3 = -\Omega_{aC}\sigma\Phi_{e^-}\left[C_{O}^{im}\right]\Delta z^3 \quad [8]$$

The volume–based etch rate has now been expressed in terms of a dissociation cross–section (equation 6) and a 2nd order rate constant (equation 8). Setting these two equations equal yields;

$$-\Omega_{aC}\sigma\Phi_{e^-}\left[C_{O}^{im}\right]\Delta z^3 = -k\left[C_{eV}\right]\left[C_{O}^{im}\right]\Delta z^3\Omega_{aC} \quad [9]$$

where Ω_{aC}, Δz^3 and $[C^{im}_O]$ disappear leaving;

$$\sigma\Phi_{e^-} = -k\left[C_{eV}\right] \quad [10]$$

with the units on each side distributed according to;

$$\left[\frac{m^2}{e^-}\right] \times \left[\frac{e^-}{m^2\,s}\right] = \left[\frac{m^3}{eV\,s}\right] \times \left[\frac{eV}{m^3}\right] \quad [11]$$

An initial inspection of equation 10 makes it difficult to rationalize a physical link between σ and k considering the introduction of time units in k. In an attempt to derive a physical meaning from equation 10, the right hand side of equation 10 will be further developed. The electron flux at the surface can be recovered on the right hand side of equation 10 using equations 3 and 4 above;

$$k\left[C_{eV}\right] = kP_d\Delta t = \frac{k\Delta t}{\Delta z}\left\{\frac{i_b}{q\Delta z^2}\left[\frac{1}{n_e}\sum_{n_e}\left(\int_{s_T}\frac{dE}{dS}ds\right)\right]\right\} = \frac{k\Delta t}{\Delta z}\Phi_{e^-} \quad [12]$$

therefore;

$$\sigma = \frac{k\Delta t}{\Delta z} \quad [13]$$

The fundamental *2nd* order rate constant applicable for the physical model used here is;

$$k = 4\pi D_{O_2}^{eff}\Delta r \quad [14]$$

where D^{eff}_{O2} is the effective diffusion coefficient which accounts for the diffusion + binding and the Δr is the radius of interaction. The form of equation 14 was derived in **S7**. This value of k was derived from the rate constant for a diffusion–limited reaction for isotropic spheres of radius

r_1 and r_2 with diffusion coefficients of D_1 and D_2 (*M. von Smoluchowski, Phys. Z 17, 557 (1916)*) where species (1) is the secondary electron and species (2) is oxygen (O_2).

The effect of secondary electrons is introduced in Δr by;

$$\Delta r = r_O + \lambda_{SE} \quad [15]$$

where r_O is the radius of bound atomic *O* and lambda is the mean free path λ_{SE} of an SE in the amorphous carbon matrix. Due to chemisorption, D^{eff}_{O2} is dominated/rate–limited by binding such that changes in the time step for magnitudes much less the binding time have a negligible effect on D^{eff}_{O2}. As a result;

$$\Delta t \cong \frac{\Delta r}{D^{eff}_{O_2}} = \frac{r_O + \lambda_{SE}}{D^{eff}_{O_2}} \quad [16]$$

and $\Delta z = \Delta r$ for this example so;

$$\sigma = \frac{k\Delta t}{\Delta z} = \frac{\left[4\pi D^{eff}_{O_2}(r_O + \lambda_{SE})\right](r_O + \lambda_{SE})}{(r_O + \lambda_{SE})D^{eff}_{O_2}} = 4\pi(r_O + \lambda_{SE})^2 \quad [17]$$

yielding a collision cross-section of form $4\pi r^2$ for a precursor molecule distributed in a 3D volume versus the traditional form of πr^2 for the collision cross-section of a precursor molecule bound at a planar, 2D surface.

Supplement 5

O_2 flux impinging on nanoparticle surfaces by diffusion

A single particle tracking, random walk Monte Carlo simulation was used to derive an expression for the oxygen impingement rate (Φ_{O2}) on the buried nanoparticle surface area as a function of nanoparticle radius $r_{np}(z,t)$ and nanoparticle site density ρ_{np}. A key assumption of the simulation was an increase in the mean nanoparticle radius (r_{np}) at constant nanoparticle site density (ρ_{np}), an assumption that is consistent with TEM observations of real samples. The input parameters for the simulation were the diffusion coefficient of molecular oxygen in the amorphous carbon matrix (D_{O2}), ρ_{np} and r_{np} for a given PtC_x composition. A simple cubic nanoparticle packing was assumed.

A simulation domain was generated with a single nanoparticle (*emulating Pt*) located at the center of a cubic domain which served as a model for the *aC*. The cubic domain had an edge length that preserved the nanoparticle site density;

$$edge = \sqrt[3]{\frac{1}{\rho_{np}}} \quad [1]$$

and was discretized into a voxel domain where the voxel edge length was selected as much smaller ($\Delta x=0.1nm$) than the nanoparticle radius. A single particle representing the O_2 molecule mimic was introduced at the unoccupied corner of the simulation domain and allowed to freely diffusive on the cubic grid of voxels (**figure S5a**). Random displacements of the particle were executed by moving the particle randomly selecting one of six possible nearest neighbor lattice positions. The time expired per displacement was linked to diffusion property and lattice spacing (Δx) via;

$$\Delta t = \frac{\Delta x^2}{6D_{O_2}} \quad [2]$$

the familiar mean squared displacement criteria for diffusion. Periodic boundary conditions were imposed at the faces of the simulation domain in order to emulate an infinite deposit. The virtual molecule was allowed to explore the domain for $N_j=50{,}000{,}000$ jumps per nanoparticle radius. This procedure was repeated for each nanoparticle radius for a vector of input sizes $\boldsymbol{r_{np}}$. The integrated number of collisions with the nanoparticle surface was collected as a function of the total number of particle displacements;

$$\frac{n_c(r_{np})}{N_j \Delta t}\left[\frac{collisions}{s}\right] \quad [3]$$

(**figure S5b**) and from this value the molecular flux at the nanoparticle surface was obtained;

$$\Phi_{O_2}(r_{np}) = \left(\frac{n_c(r_{np})}{N_j \Delta t}\right)\frac{1}{4\pi r_{np}^2} \quad [4]$$

The functional behavior of Φ_{O2} vs r_{np} was well fit using a 2nd order polynomial;

$$\Phi_{O_2}(r_{np}) = C_1 r_{np}^2 + C_2 r_{np} + C_3 \quad [5]$$

and the result of this fit is shown in **figure S3c**. Importantly, the concentration of the test particle in each simulation is a function of the nanoparticle radius because the nanoparticle itself occupies a portion of the available volume;

$$C_{O_2}^{ref}(r_{np}) = \frac{1}{\sqrt[3]{\frac{1}{\rho_{np}}} - \frac{4\pi r_{np}^3}{3}} \quad [6]$$

since the nanoparticle volume increases for a fixed simulation domain size. In concert, equations 5 & 6 are later used in a calculation that determines the chemisorption of oxygen at the nanoparticle surfaces as a function of depth into the deposit.

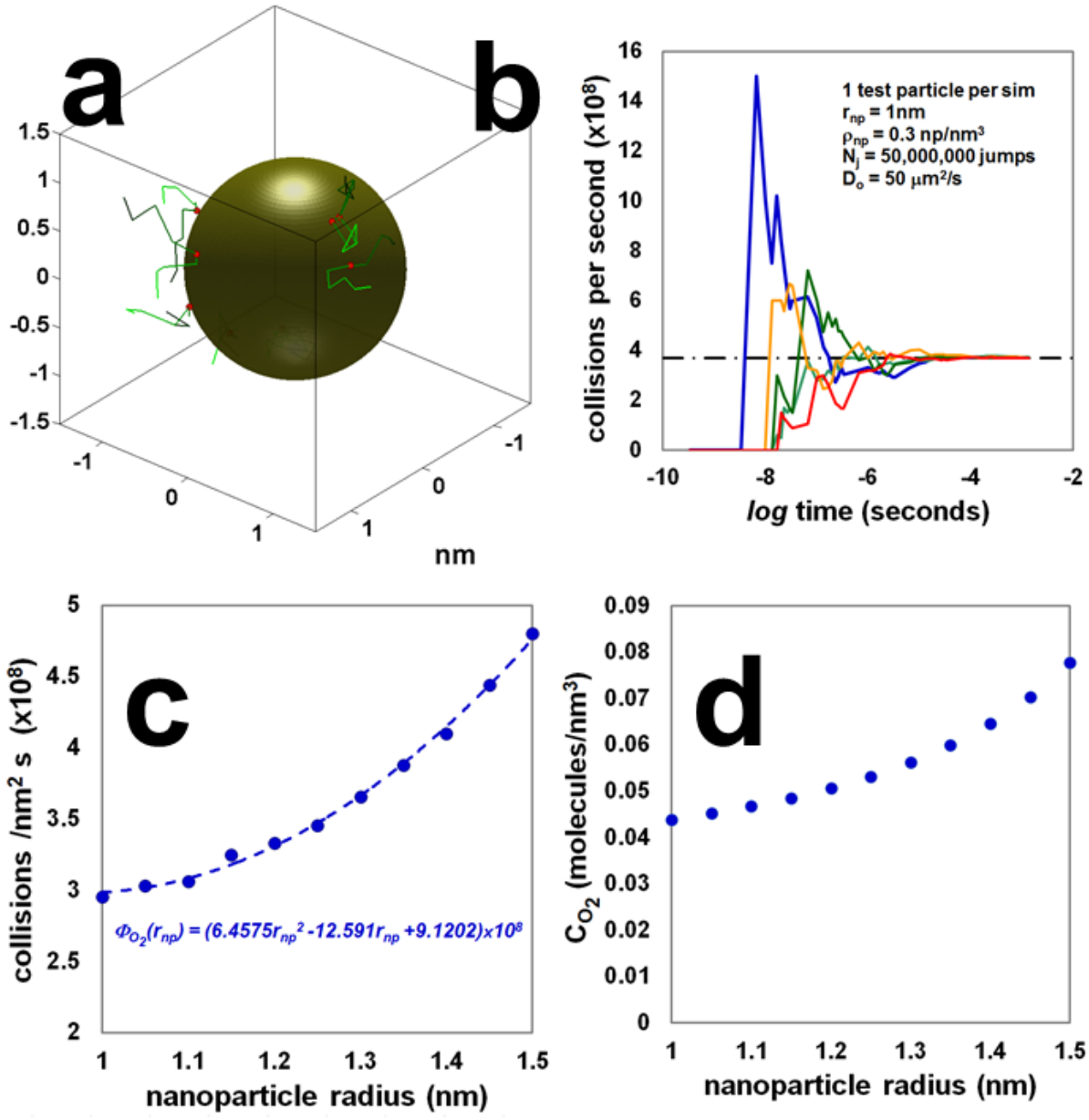

Figure S5 (a) Multiple time snapshots of a single virtual particle trajectory (emulating diffusing O_2) during select periods of interaction with the nanoparticle surface (emulating a Pt nanoparticle). A total of 10 snapshots are shown, each lasting 1.67ns. The trajectory shading shows the initial position of the snapshot (black) to the end at 1.67ns (green). The moment of collision between the diffusing virtual particle and the nanoparticle is shown as a red circle. Ten random collision events were selected for display. (b) The particle tracking simulation converges to the particle impingement rate at large numbers of simulated jumps for a single diffusing particle. Specifically, the mean impingement rate is calculated as the total number of collisions divided by the total elapsed simulation time and the nanoparticle surface area. A host of simulations were executed varying the nanoparticle radius in order to calculate the impingement rate as a function of the nanoparticle radius. 50,000,000 jumps are executed per simulation. In this example, five identical computer experiments are shown for a fixed nanoparticle radius of 1nm in a simulation domain with an edge length of ~3nm. Notice the x–coordinate is log time and the computer experiment extends over 7-orders of magnitude in time up to the millisecond time scale. The random

nature of diffusion at the shortest time scales is evident but convergence is obtained at the millisecond time scale yielding a collision rate of $3.8 \times 10^{+8}$ collisions per second for all 5 computer experiments. Thus, this value represents the molecular impingement rate, by diffusion, on the nanoparticle surface area (c) The results for multiple radii are shown (each data point was generated by one computer experiment such as that shown in (b). The collision frequency increases as the nanoparticles grow because (1) the surface area of the nanoparticle increases yet (2) the (d) effective concentration is increasing for the each test simulation because the unoccupied volume is decreasing for the test particle. The diffusion-based impingement is derived from these results taking into account the reference concentration used for each simulation.

Supplement 6

Transient nanoparticle growth within the deposit

Pt nanoparticle growth was found to occur during real purification experiments. The model presented here for purification assumes that O_2 must exhibit dissociative absorption for the oxidation reaction to occur. Therefore, the available nanoparticle area per pixel is an important variable in the simulation and the method to account for this parameter is described below.

The nanoparticle density (ρ_{np}) and the mean nanoparticle radius in the initial deposit ($r_{np(i)}$) are used to determine the starting volume of platinum per voxel;

$$V_{Pt} = \Delta x^3 \rho_{np} \frac{4}{3} \pi r_{np(i)}^3 \quad [1]$$

and Δx^3 is the initial voxel volume. These are the required initial conditions in order to later account for O_2 binding at nanoparticle surfaces. Each deposit voxel is partitioned into two mathematical phases (1) pure *Pt* and (2) amorphous carbon (*aC*). First, the term "*mathematical phase*" is used to signify that the nanoparticles do not have an actual spatial representation in the simulation but rather that a mean nanoparticle radius is calculated depending on the change in pixel size as *aC* is liberated. We assume a simple cubic arrangement of nanoparticles in the following mathematical development for simplicity as the packing of nanoparticles is a weakly influential parameter in the simulation. Importantly, the mathematical development here is performed in terms of a voxel implying a volume, i.e., three dimensions, but the final result below will ultimately be 1D which is compatible with the 1D transport simulation used to emulate the O_2 reaction–diffusion. Lastly, V_{Pt} is held constant during the simulation and purification ensues by a relative enrichment per pixel of *Pt*–to–*aC*. The model for nanoparticle growth follows in light of these initial conditions, features and assumptions.

The nanoparticle surface area (σ_{np}) as a function of time per voxel is;

$$\sigma_{np}(z,t) = V(z,t) \rho_{np} 4\pi r_{np}(z,t)^2 \quad [2]$$

and the volume per voxel is time–dependent;

$$V(z,t) = \Delta x^2 \Delta z(t) \quad [3]$$

V_{Pt} is constant and $\Delta z(t)$ is calculated directly from the simulation which makes it possible to solve for $r(z,t)$ using equations 1 & 3 yielding;

$$r_{np}(z,t) = r_{np(o)} \sqrt[3]{\frac{\Delta x}{\Delta z(t)}} \quad [4]$$

where the radius of the nanoparticles increases as *aC* is liberated. Remember from above that the nanoparticle density per pixel (ρ_{np}) has been set as a constant. However, within the context

of the proposed model of a fixed V_{Pt} coupled with a shrinking pixel thickness, the nanoparticle density should increase as the pixel shrinks with a constant nanoparticle size during the simulation. Therefore, the mathematical approach presented above makes it possible via the conservation of *Pt* volume per pixel to vary the nanoparticle radius at constant ρ_o while maintaining the computational advantage of a fixed V_{Pt} with a shrinking pixel size. Lastly, it was initially enticing to model the nanoparticle growth process simply as an Ostwald ripening process. The Ostwald ripening [1] equation is provided here;

$$\langle R\rangle^3 - \langle R\rangle_o^3 = \frac{8\gamma C_\infty v^2 D}{9R_g T}t \quad [5]$$

where <*R*> is the average radius of the nanoparticle distribution, γ is the nanoparticle surface energy, C_{inf} is the solubility of the nanoparticle, v is the molar volume, D is the diffusion coefficient of the *Pt* nanoparticles, R_g is the gas constant, T the temperature and t the time. However, the loss of *aC* causes a deposit contraction which also acts to bring relatively small nanoparticles into contact. Thus, without detailed experimental knowledge regarding the transient nature of the nanoparticle morphology it was decided to use the more simple approach presented in this Supplement.

[1] W. Ostwald. **1896**. *Lehrbuch der Allgemeinen Chemie*, vol. 2, part 1. Leipzig, Germany.

Supplement 7

Parameter ranges

Diffusion coefficient of O_2 in aC (D)

A search range of 10^{-2}–10^{+1} $\mu m^2/s$ was selected for the diffusion coefficient. This range was suggested by a plot of provided in [1] for a carbon matrix with glassy polymer properties. For polymeric materials, the diffusion coefficient can be as high as *100–200* $\mu m^2/s$ but simulations using these relatively high value of *D* didn't replicate experimental findings and these relatively higher values are commonly associated with polymers that have a more "rubbery" character.

[1] *Materials Science of Membranes for Gas and Vapor Systems*, Eds., Y. Yampolskii, I. Pinnau and B. D. Freeman 2006 John Wiley & Sons, Ltd.

Sticking coefficient of O_2 on Pt

The sticking coefficient of oxygen gas onto platinum surfaces was taken as *0.05* based on [2] which is low coverage value [7]. As stated in the main text, this value applies for vapor phase O_2 impinging on exposed *Pt* surfaces whereas we are extrapolating the use of this parameter to dissolved O_2 impinging on buried *Pt* and the validity of this assumption is unknown.

[2] D. R. Monroe and R. P. Merrill, "Adsorption of Oxygen on Pt(111) and Its Reactivity to Hydrogen and Carbon Monoxide", *Journal of Catalysis* **65**, 461 (1980)

[7] C. T. Campbell, G. Ertl, H. Kuipers and J. Segner, "A Molecular Beam Study of the Adsorption and Desorption of Oxygen from a Pt(111) Surface", *Surface Science* **107**, 220 (1981)

Binding site density of O on Pt nanoparticle surface area

Reference [2] also reports 1 oxygen atom adsorbed per 4 *Pt* atoms on the (*111*) surface at saturated coverage. An oxygen surface site density was estimated from this information according to;

$$s_d = \frac{21.1\left[\frac{g}{cm^3}\right]6.02x10^{23}\left[\frac{atoms}{cm^3}\right]0.25\left[\frac{O}{Pt\ atom}\right]}{195.1\left[\frac{g}{mol}\right]1x10^{21}\left[\frac{nm^3}{cm^3}\right]} = 16\frac{O}{nm^2} \cong 8\frac{O}{nm^2}$$

and where the average *Pt* density was used instead of the *Pt(111)* planar density and the value used here of 8 O/nm^2 reflects the fact that the total nanoparticle surface area exposes an average planar density less than the most densely packed (111) plane.

Adsorption energy of O & H_2O on Pt

The adsorption energy for O_2 on pure *Pt* surfaces is reported as ~(*-4eV*) in [3]. This yields a mean residence time of *~Inf* for the lifetime of *O* on *Pt* relative to the time expired during real purification experiments executed at *298K*. H_2O on the otherhand, has an adsorption energy of ~(*0.3eV*) [3-4] which yields picosecond adsorption times at *298K*. Thus, for the H_2O, adsorption on *Pt* surfaces may be neglected in simulations. Similarly, [5] reports a bond enthalpy for *X-Pt* of *~3eV/atom* for *O* and *~0.3eV/atom* for H_2O. Campbell has reported [7-8] -2.8eV/atom on Pt thin films.

[3] G. S. Karlberg, "Adsorption trends for water, hydroxyl, oxygen and hydrogen on transition–metal and platinum–skin surfaces", *Physical Review B* **74**, 153414 (2006)

[4] S. Meng, E. G. Wang and S. Gao, "Water adsorption on metal surfaces: A general picture from density functional theory studies", *Physical Review B* **69**, 195404 (2004)

[5] E. M. Karp, C. T. Campbell, F. Studt, F. Abild – Pedersen and J. K. Norskov, "The energetics of oxygen adatoms, hydroxyl species and water dissociation on Pt(111), *Journal of Physical Chemistry C* **46**, 25772 (2012).

[8] D. Brennan, D. O. Hayward and B. M. W. Trapnell, "The Calorimetric Determination of the Heats of Adsorption of Oxygen on Evaporated Metal Films", *Proceedings of the Royal Society (London) A* **256**, 81 (1960)

Permeability coefficient of O in glassy polymers

The permeability coefficient at STP for a host a polymers is listed in [6] ranging from $1x10^{-13}$ - $1x10^{-16}$ (*cm³ STP*)(*cm*)/(*cm² s Pa*). Reference [1] provides a range of $1x10^{-17}$ – $1x10^{-9}$. Glassy polymers capable of including a relatively large void fraction can have permeability coefficients as high as $1x10^{-10}$ (*cm³ STP*)(*cm*)/(*cm² s Pa*) [7]. Therefore, the range explored for a solution was $1x10^{-10}$–$1x10^{-16}$ (*cm³ STP*)(*cm*)/(*cm² s Pa*).

[6] W. D. Callister and D. G. Rethwisch, "Materials Science and Engineering: An Introduction", Version 9E, pg. 572 (2014)

[7] J. C. Salamone, "Polymeric Materials Encyclopedia", Volume 9, Edition 12, pg. 6762 (1996)

Reaction rate constant (k)

Summary

The 2nd order reaction rate constant for a pair of interacting, mobile species in solution is provided below. The empirical reaction rate law treatment implemented in the model, i.e., $k[C_{eV}][C_O]$, suggests that the simulation results should be consistent with the fundamental derivation of the rate constant as provided in equation 1 below. The aim of this supplement is to report the physically meaningful range for k and to test the consistency of simulation results with experiments. A value of $k = 4x10^{+3}$ $nm^3/eV/s$ predicted well experimental results for the purification of PtC_5 with O_2. The effective diffusion coefficient D_{O2}^{eff} is a meaningful parameter in the analysis of k. The k value derived from simulations was tested by rearranging equation 1 to solve for the interaction radius which should yield a result that lies between the radius of molecular oxygen (~0.3nm) and the radius of the nanoparticle + the electrons effective radius (taken as the maximum SE range; ~2.5nm). This was indeed the case. Finally, the value of k reported falls within the range dictated by coupling to the diffusion coefficient range of 0.1–10 nm^2/s: because the binding interaction is strong, this interaction dominates transport and $D_{O2}^{eff} = 350nm^2/s$ for both 0.1 and 10 $\mu m^2/s$. As a result, the range of k depends on the physically relevant radius values, e.g., $k = 4\pi x350[nm^2/s]0.3[nm] - 4\pi x350[nm^2/s]x2.5[nm] = 1320 - 11000\ nm^3/e^- s$, or $k = 220 - 2200\ nm^3/eV/s$ assuming 5eV per SE. Further details are provided below.

The reaction rate constant for a binary mixture of mobile particles is;

$$k = 4\pi(D_1 + D_2)(r_1 + r_2) \quad [1]$$

where the subscripts *1* & *2* identify the two species of interest which are electrons and molecular oxygen, *D* is the diffusion coefficient and *r* is the molecular radius. Inserting the variables of interest here yields

$$k = 4\pi D_{O_2}^{eff}\left(r_{O_2} + r_{eV}\right) \quad [2]$$

The focused electron beam (~25nm) is significantly larger than the radius of a nanoparticle (~1nm) which only enlarges due to elastic electron scattering into the bulk. As a result, the 'diffusion' of electrons is not rate limiting for the electron beam–induced dissociation process because the electron energy loss falls uniformly over the nanoparticle surface area for relatively large primary beam currents on the order of pA–nA that act to uniformly impinge the beam area after a large number of random impacts. Thus, D_{eV} was removed from the expression

The effective diffusion for molecular oxygen is the relevant variable here because the dissociative chemisorption–associative desorption ultimately impacts the diffusion property from the point-of–view of equation 1. Moreover, it is bound atomic oxygen that is dissociated by the electron beam with high probability. In order to estimate the effective diffusion coefficient, the single particle tracking simulation described in **S5** was further developed to include the binding/unbinding of the particle at the embedded nanoparticle surface (**figure S7**)

In this binding + diffusion regime the effective diffusion coefficient (D^{eff}_{O2}) is the relevant parameter for application in equation 2. The relatively long mean residence time (τ) of *12.5ms* strongly affects the effective diffusion property as was confirmed using the single particle tracking Monte Carlo simulation described above with the addition of the following features.

The single tracking particle simulation was modified to account for binding. On impact with the nanoparticle surface, a binding test was executed based on the sticking probability (δ) and the current oxygen coverage (θ)

$$rand < \delta(1-\theta) \quad [2]$$

rand is a random number spanning the range *0–1* and θ spans the same range for monolayer coverage. A randomly sampled residence time was generated and added to the lapsed simulation time if the binding test was satisfied. The random residence time was determined by;

$$t_{bound} = -\tau \ln(rand) \quad [3]$$

The particle is then released from the nanoparticle surface and allowed to freely diffuse after the addition of the randomly sampled residence time t_{bound}. **Figure S5** shows the results of including the binding interaction on the particle mean squared displacement as a function of time. The free diffusion coefficient of 4,000,000 nm^2/s is reduced to D^{eff}_{O2}=350 nm^2/s due to the binding interaction.

Rearranging equation 1 and inserting values derived from the 5keV, 1800pA simulation;

$$r_{eV} + r_{np} = r_i \cong \frac{k}{4\pi D_{eff}} = \frac{4000\left[\frac{nm^3}{eV\ s}\right]}{4 \times \pi \times 350\left[\frac{nm^2}{s}\right]} = 0.9\left[\frac{nm}{eV}\right] \quad [4]$$

where r_i is the interaction radius. The energy loss in equation 4 is converted to a per electron basis using a mean SE electron energy of 5eV/SE assuming that the energy loss pathway to secondary electrons drives the electron–induced surface reaction with bound atomic O on the Pt nanoparticles;

$$0.9\left[\frac{nm}{eV}\right] x\ 5\left[\frac{eV}{e^-_{SE}}\right] = 4.5\ nm$$

This result is considered promising as it agrees with what be expected from the summation of the nanoparticle radius and the mean free path of an excited SE electron which typically falls in the range of 0.5–3nm.

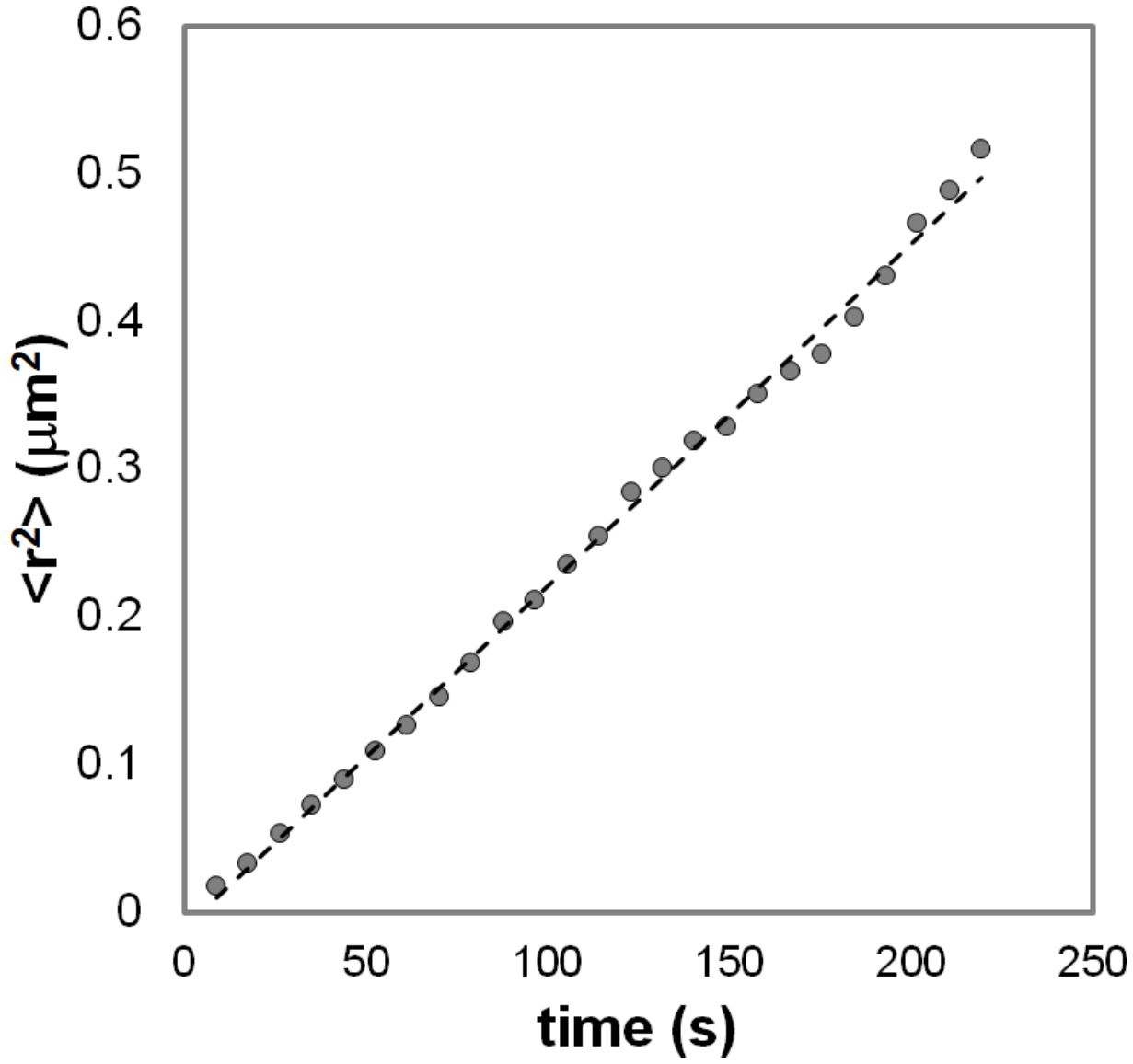

Figure S7 The mean squared displacement $\langle r^2 \rangle$ vs elapsed time for a single particle that is executing random diffusive motion on a square lattice. A portion of the free lattice volume is occupied by a single nanoparticle according to a nanoparticle site density of $3.25 \times 10^{-2}/nm^2$, a nanoparticle radius of 1nm and a simple cubic lattice. The simulation domain edge length is chosen to preserve the nanoparticle site density (**see S5**). The single particle has a binding probability to the nanoparticle surface defined by a sticking probability of 0.05 and a mean residence time of 12.5ms. 50,000,000 displacements were executed per particle in order to

generate a $\langle r^2 \rangle$ vs time trace. A total of 250 independent computer experiments were executed and averaged in $\langle r^2 \rangle$ to generate the data points (circles). A linear fit to the data yields a slope equal to $6*D_{eff}$ according to $\langle r^2 \rangle = 6Dt$, in this case, yielding $D_{eff} = 350\ nm^2/s$.

Supplement 8

Diffusion coefficient – reaction constant – solubility parameter space

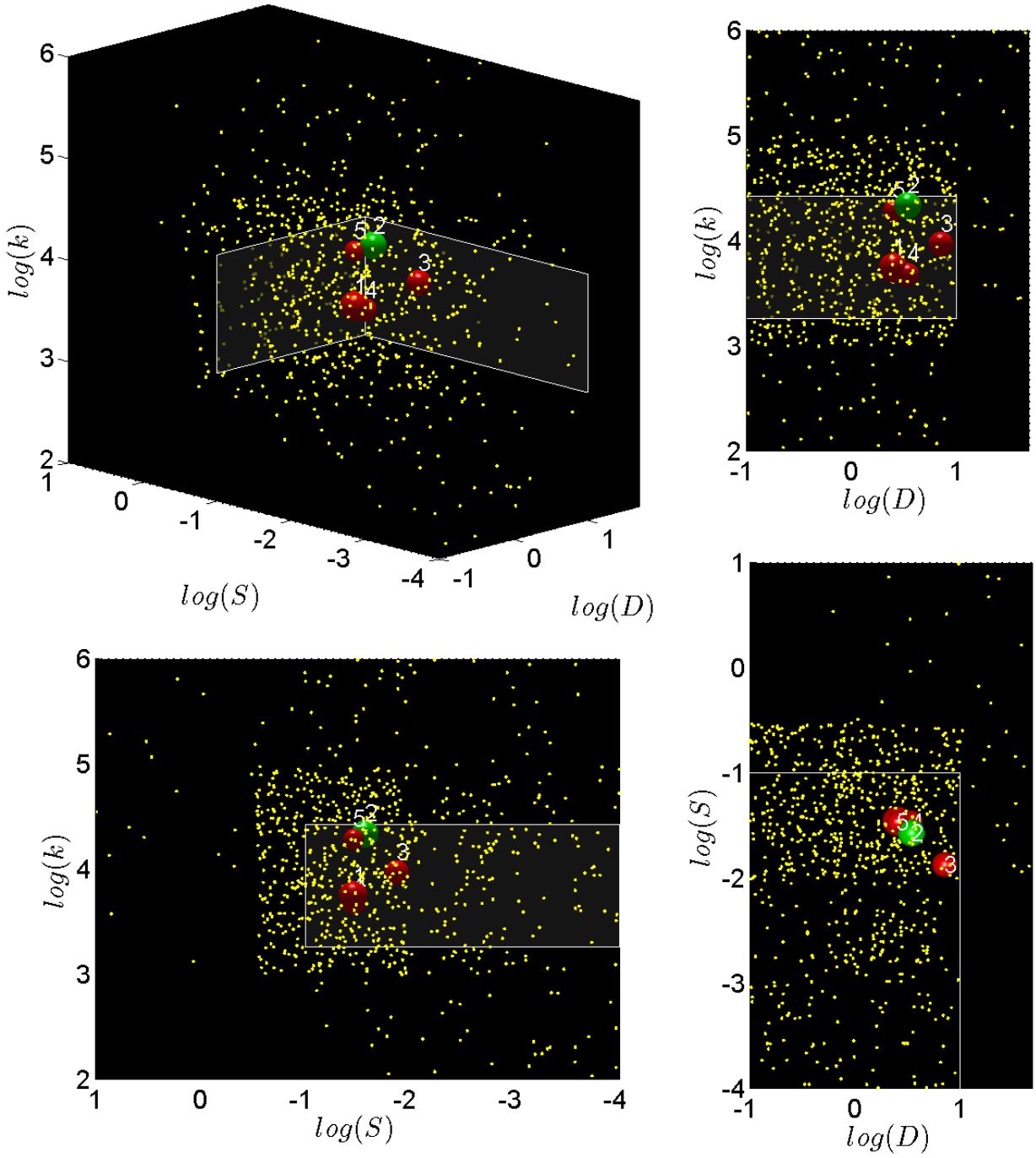

Figure S8 (a) A space map of simulation parameters. The 3D space has coordinates of mobile oxygen gas diffusion coefficient (D), solubility parameter (S) and the reaction constant (k). The axes are displayed in log_{10}. Each white dot in space represents a single purification loop experiment for the 5keV O_2 experimental condition provided in the **Table S1**. Realistic solutions are confined to the region in space defined by the two superimposed planes; the S-k plane at D_o = 10 μm^2/s where realistic solutions fall within D_o < 10 μm^2/s and the D_o-k plane at S=0.1 molecules/nm^3/Torr for all solutions lying within S<0.1 molecules/nm^3/Torr. Five of the

ten best solutions fell within the indicated range and are indicated by spheres. Red spheres indicate contraction rates less than the experiments and green indicates contraction rates greater than that observed in experiments. The relative size of the sphere indicates solution quality – the best solution has the larger sphere diameter and is also labeled with '1' clarity. (b-d) Parameter space map views highlighting all possible combinations of binary parameter pairs.

Supplement #9

Polymer-like amorphous carbon (aC) permeability coefficient

An aspect of the model for electron beam driven purification considered that O_2 dissolved in the *aC* phase of the *PtCx* deposit. This model was chosen based on previous reports of the polymer–like nature of the *aC* in EBID deposits. An O_2 solubility in *aC* of $S \approx 10^{-2}$ *molecules/(nm³ Torr)* yielded simulation results that were consistent with experimental purification rates and the PtC_x final composition. In order to test the assumption of a polymer–like *aC* phase the reported solubility is converted into a permeability coefficient (Π) in order to compare with literature values reported for similar polymers. The permeability coefficient is related to the *S* via;

$$\Pi = D_{O_2} S \quad [1]$$

and D_{O2} is the diffusion coefficient of O_2 in *aC*. A diffusion coefficient on the order of 10^6 nm²/s yields a permeability coefficient of;

$$\Pi \cong 10^4 \left[\frac{nm(molecules)}{nm^2 Torr\ s}\right] \quad [2]$$

In order to make an easier comparison with values reported in the literature the units are changed

$$\Pi = 10^4 \left[\frac{nm(molecules)}{nm^2 Torr\ s}\right] \ \frac{760\ Torr\ \ 10^7 nm}{101325\ Pa\quad cm} = 7.5x10^8 \left[\frac{cm(molecules)}{cm^2 Pa\ s}\right] \quad [4]$$

and the permeability is expressed at STP (298K, 1cm³, 1atm) as;

$$n(1atm, 1cm^3, 298K) = \frac{(101325Pa) \times (1cm^3)}{\left(8.314 \frac{J}{mol\ K}\right) \times (298K)} \cdot \frac{10^{-6} m^3}{cm^3} \cdot \frac{6.02x10^{23} molecules}{mol} \quad [5]$$

$$\Pi = 7.5x10^8 \left[\frac{cm(molecules)}{cm^2 Pa\ s}\right] \times \frac{(cm^3 STP)}{2.462x10^{19}} \cong 10^{-11} \left[\frac{cm(cm^3 STP)}{cm^2 Pa\ s}\right] \quad [6]$$

This value is characteristic of the upper limit of the permeability coefficient reported for typical polymeric materials. The higher simulated permeability may be due to the porosity common in EBID deposits which has been shown to increase the effective solubility of dissolved gases and in commonly interpreted within the context of the dual sorption model.

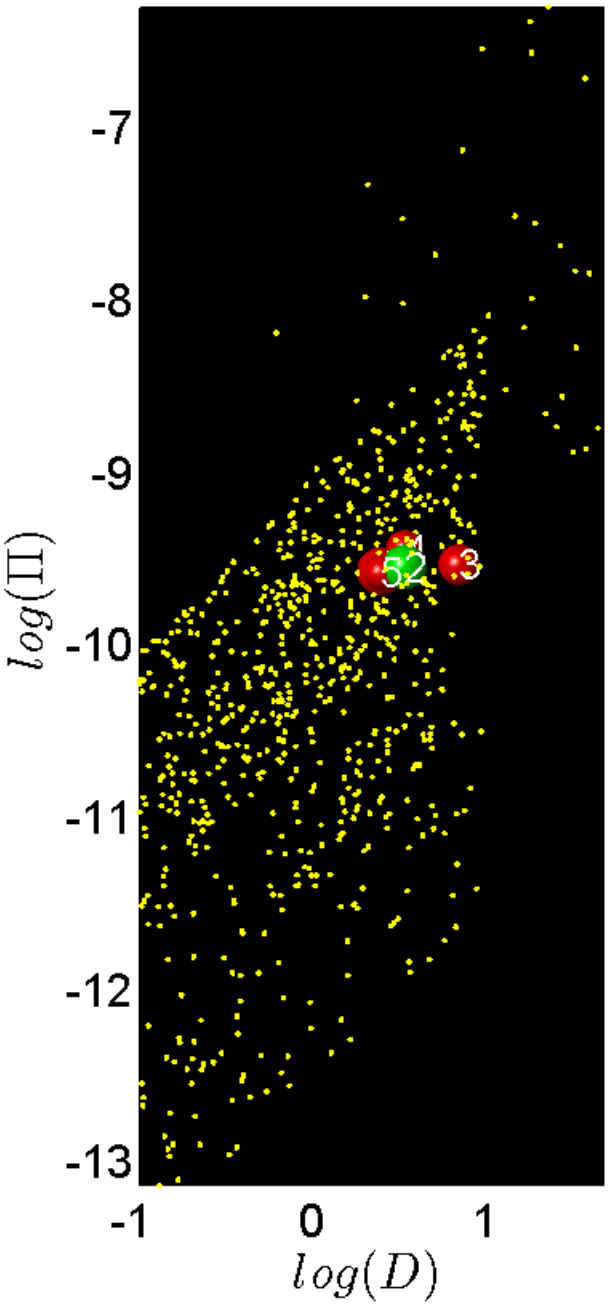

Figure S9 A view of the (Π–D_o) solution plane.

Supplement #10

Simulation diagram

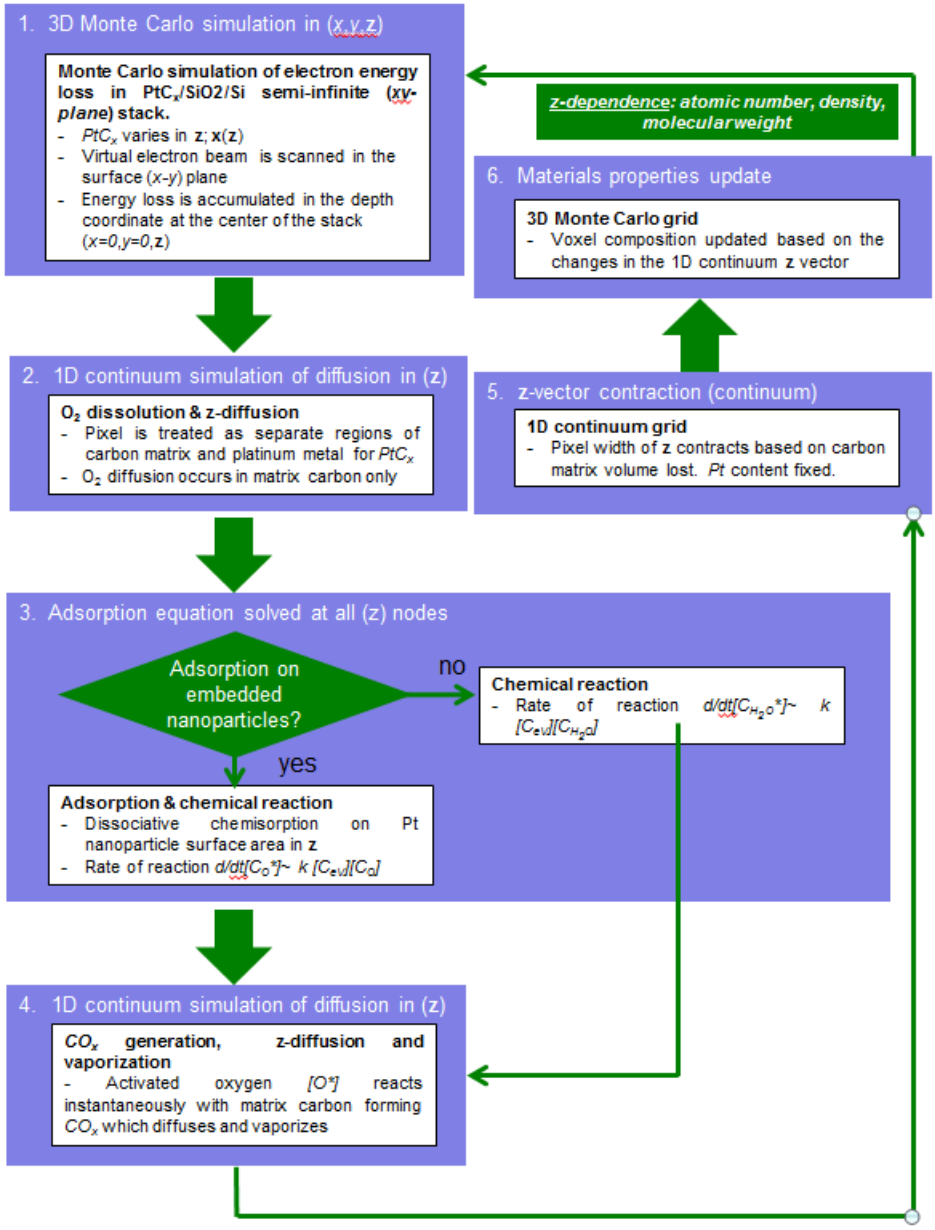

Figure S10 Computational flow diagram for a single purification loop. The physical chemistry aspects and the transient nature of the materials properties have been specified.